Applied Catalysis B: Environmental 129 (2013) 403–408

Contents lists available at SciVerse ScienceDirect

Applied Catalysis B: Environmental

journal homepage: www.elsevier.com/locate/apcatb

A promising new photocatalyst $CdSnO_3 \cdot 3H_2O$ for air purification under ambient condition

Yibin Chen[a,b], Danzhen Li[a,*], Jing Chen[a], Jinxiu Wang[a], Sugang Meng[a], Jiangjun Xian[a], Xianzhi Fu[a], Yu Shao[a]

[a] Research Institute of Photocatalysis, State Key Laboratory Breeding Base of Photocatalysis, Fuzhou University, Fuzhou, Fujian 350002, PR China
[b] Department of Biological and Chemical Engineering, Fuqing Branch of Fujian Normal University, Fuzhou, Fujian 350300, PR China

ARTICLE INFO

Article history:
Received 27 June 2012
Received in revised form
16 September 2012
Accepted 19 September 2012
Available online 27 September 2012

Keywords:
$CdSnO_3 \cdot 3H_2O$
Photocatalysis
Homogenous precipitation
Volatile organic compounds

ABSTRACT

A new binary metal hydrate photocatalyst $CdSnO_3 \cdot 3H_2O$ was synthesized from $Cd(CH_3COO)_2$ and $SnCl_4 \cdot 5H_2O$ via a facile homogenous precipitation method. The photocatalytic activities of samples were evaluated by the photocatalytic degradation of volatile organic compounds (VOCs) in O_2 gas stream under ultraviolet light irradiation. The results demonstrated that the typical $CdSnO_3 \cdot 3H_2O$ sample had an average particle size of about 16 nm, a band gap of 4.4 eV, and a specific surface area of 91.8 $m^2 g^{-1}$. The comparison of $CdSnO_3 \cdot 3H_2O$ synthesized at different pH values showed that the photocatalytic activities of $CdSnO_3 \cdot 3H_2O$ synthesized at pH 7 and 8 were higher than that of the samples synthesized at pH 6 and 9. Contrast to commercial P25-TiO_2, the activity of this new photocatalyst was better. The conversion ratio of benzene was about 45% and 5%, corresponding to the mineralization ratio was about 60% and 25%, respectively. $CdSnO_3 \cdot 3H_2O$ also exhibited high photocatalytic activities towards cyclohexane and acetone. Then, the mechanism of the reaction on the new photocatalyst was discussed. Hence, the facile synthesis of this photocatalyst and its outstanding photocatalytic performance for VOCs are favorable to its potential application in the environmental remedy field.

1. Introduction

The photocatalytic oxidation (PCO) technology based on TiO_2 is a environmentally and friendly, ambient reaction and wide-adaptability of organic pollutants in the environmental remediation [1,2]. Although numerous volatile organic compounds (VOCs) can be photo-degraded to CO_2 and H_2O by TiO_2, the PCO technology in the treatment of aromatic compounds like benzene is limited, due to the deactivation of TiO_2 resulting from the accumulation of some stable reaction intermediates on the surface [3,4]. Further studies were going on last decades. Some made efforts on catalyst modification [5,6]. Another studies on establishing the complicated hybrid system such as adding water vapor [7,8] into the reaction system showed that it could improve the photodegradated efficiency of benzene at ambient conditions. But it is not easy to realize the practical application of air purification. So, the development of new photocatalyst with high performance for refractory organics is indispensable.

The development of new photocatalysts has been a very active research topic. The typical non-titania photocatalysts such as vanadates [9–11], metal oxide [12], and binary metal oxide [13] were reported. Recently, the studies on perovskite-type stannates showed that the stannates presented high photocatalytic activity toward dyes in water [14,15]. And it is worth mentioning that, the photocatalysis of zinc hydroxystannate (ZHS) was reported and the high activity of ZHS was mainly attributed to the abundance of surface OH groups which accepted photogenerated holes to yield highly reactive •OH radicals [16]. Other metal hydrates with high photocatalytic performance have been proved in our lab, such as $In(OH)_3$ [17], InOOH [18] and $CaSb_2O_5(OH)_2$ [19]. Those stimulate our interest to further investigate whether the other hydrates have high photoactivity or not. For zinc and cadmium were group IIB element, the structure of cadmium hydroxystannate would be similar to that of $ZnSn(OH)_6$ (Fig. S1), and the study on cadmium hydroxystannate is very few. Previously, uniform crystalline $CdSnO_3 \cdot 3H_2O$ nanocubes with 28–35 nm edge length had been obtained via the ion exchange reaction of $Na_2Sn(OH)_6$ in $CdSO_4$ aqueous solution, assisted by ultrasonic treatment [20]. To the best of our knowledge, there are no report on the homogenous precipitation synthesis of $CdSnO_3 \cdot 3H_2O$ nanoparticles and its application in photocatalysis. Herein, a feasible one-step synthesis of $CdSnO_3 \cdot 3H_2O$ nanoparticles via homogenous precipitation and its high photocatalytic activity on volatile organic compounds were reported. The related properties of $CdSnO_3 \cdot 3H_2O$ were discussed, and a possible mechanism

* Corresponding author. Tel.: +86 591 83779256; fax: +86 591 83779256.
E-mail address: dzli@fzu.edu.cn (D. Li).

0926-3373/$ – see front matter © 2012 Elsevier B.V. All rights reserved.
http://dx.doi.org/10.1016/j.apcatb.2012.09.030

of the new photocatalyst with high photocatalytic activity towards VOCs was proposed.

2. Experimental

2.1. Homogenous precipitation synthesis of $CdSnO_3{\cdot}3H_2O$

All of the reagents were analytical grade and were used without further purification. The $CdSnO_3{\cdot}3H_2O$ was prepared by homogenous precipitation using $Cd(CH_3COO)_2$ and $SnCl_4{\cdot}5H_2O$ as starting materials. In a typical synthesis, 1.20 g of sodium hydroxide was dissolved in 75 mL of $SnCl_4$ (0.1 mol L^{-1}) aqueous solution at room temperature. Then 75 mL of $Cd(CH_3COO)_2$ (0.1 mol L^{-1}) was mixed with above aqueous solution. The pH values of the mixed solutions were adjusted at 6–9 by adding 2 mol L^{-1} HCl or 2 mol L^{-1} NaOH. The mixed aqueous solutions were stirred. And then the products were separated from the white slurry by centrifugation. The obtained samples were repeatedly washed with distilled water and alcohol to remove excess salts and were dried at 60 °C in air.

2.2. Characterizations of photocatalyst

The X-ray diffraction (XRD) patterns of the samples were performed on a Bruker D8 Advance X-ray diffractometer with Cu Kα radiation. The transmission electron microscopy (TEM) and high-resolution transmission electron microscopy (HRTEM) images were measured by a JEOL model JEM 2010 EX instrument at an accelerating voltage of 200 kV. The UV–vis diffuse reflectance spectrum (DRS) was recorded on a Varian Cary 500 Scan UV–Vis–NIR spectrometer with $BaSO_4$ as the background between 200 and 800 nm. The nitrogen adsorption–desorption isotherm was collected at 77 K using OMNISORP100CX equipment. The specific surface area was calculated using the Brunauer–Emmett–Teller (BET) method. The sample was degassed at 130 °C and 10^{-6} Torr for 5 h prior to the measurement. The X-ray photoelectron spectroscopy (XPS) analysis was conducted on an ESCALAB 250 photoelectron spectroscopy (Thermo Fisher Scientific) at 3.0×10^{-10} mbar with monochromatic Al Kα radiation. The electron spin resonance (ESR) signals of the radicals spin-trapped by 5,5-dimethyl-l-pyrroline-*n*-oxide (DMPO) were recorded with an EPR spectrometer (ESP 300E, Bruker). A spot UV-light source of Hamamatsu Co. (LC8) (equipped with a 254 nm filter) was used as a photo-excitation light source.

2.3. The test of photocatalytic performance

The photocatalytic oxidation experiments of VOCs were operated in a tubular quartz microreactor with a continuous-flow mode. The quartz vessel was surrounded by four 4 W fluorescent UV bulbs (TUV 4W/G4 T5, Philips, wavelength 254 nm). The vessel is 11 cm in length and 2.4 mm in diameter, in which only 0.3 g of catalyst (50–70 mesh) was loaded. The vessel is narrow and the UV light was irradiated from four directions (as was shown in Fig. S2). Thus, the photocatalyst bathe in the UV light. Diluted benzene, cyclohexane or acetone vapor (280 ± 20 ppm) was introduced into the reactor along with a continuous O_2 gas stream with a total flowrate of 20 cm^3 min^{-1}. Prior to irradiation, the adsorption–desorption equilibrium of VOCs on the photocatalyst was carried out for 12 h, which is balanceable concentration of VOCs was maintained at about 280 ± 20 ppm and CO_2 was zero. During the photocatalytic degradation process, the temperature of the reaction was maintained at temperature at 35 ± 1 °C, which was effectively controlled by an air-cooling system. The concentrations of VOCs and CO_2 were analyzed by an on-line gas chromatograph (HP6890), equipped with a thermal conductivity detector, a flame ionization detector, and a Porapak R column. The conversion and mineralization of benzene for reaction are calculated using following equations:

$$\%\ \text{conversion} = \frac{[C_6H_6]_{\text{converted}}}{[C_6H_6]_{\text{total}}} \times 100 \quad (1)$$

$$\%\ \text{mineralization} = \frac{[CO_2]_{\text{produced}}}{6[C_6H_6]_{\text{converted}}} \times 100 \quad (2)$$

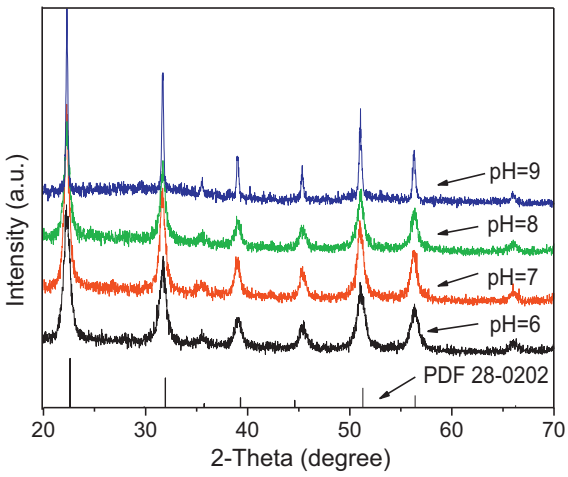

Fig. 1. XRD patterns of the samples prepared via co-precipitation at different pH.

3. Results and discussion

3.1. Characterization of the catalysts

The XRD patterns of $CdSnO_3{\cdot}3H_2O$ samples synthesized at different pH values were shown in Fig. 1. All the diffraction peaks of these samples were in line with the standard spectrum (JCPDS no. 28-0202). Distinctive peaks at 22.30°, 31.70°, 39.08°, 51.09°, and 56.38° were matched well with the (2 0 0), (2 2 0), (2 2 2), (4 2 0) and (4 2 2) crystal planes of cubic $CdSnO_3{\cdot}3H_2O$. According to the Scherrer formula, the average particle sizes of $CdSnO_3{\cdot}3H_2O$ synthesized at pH of 6, 7, 8 and 9 were about 12.5, 16.8, 15.5, and 41 nm, respectively.

The morphology of $CdSnO_3{\cdot}3H_2O$ prepared at pH 7 was investigated with TEM. The TEM images of as-prepared sample Fig. 2a showed that most of the as-prepared $CdSnO_3{\cdot}3H_2O$ particles were nanocubes and their edge length was in the range of 10–20 nm. The HRTEM image (Fig. 2b) revealed the interlayer spacing of 0.274 nm corresponding to the (2 2 0) plane of as-prepared $CdSnO_3{\cdot}3H_2O$.

Fig. 3 showed the UV–vis diffuse reflectance spectra of $CdSnO_3{\cdot}3H_2O$ nanoparticles. The sample represented a photo absorption property in the UV light region. It is well-known that the relation between absorption coefficient and band gap energy of an direct gap semiconductor can be described by the formula $[F(R)E]^2 = A(E - E_g)$, where E and E_g are the photon energy and optical band gap energy, respectively, and A is the characteristic constant of semiconductor [21]. In the equation, $[F(R)E]^2$ has a linear relation with E. Extrapolating the linear relation to $[F(R)E]^2 = 0$ could get the band gap E_g of the sample. So the band gap of $CdSnO_3{\cdot}3H_2O$ synthesized at pH 7 was calculated approximately to be 4.4 eV and the absorption edge of the sample was located at 281.8 nm (as shown in Fig. 3). The band gaps of other samples prepared at pH 6, 8, and 9 were calculated in the same way, corresponding to 4.5, 4.3, and 4.1 eV, respectively (as shown in Fig. S3).

Fig. 4 showed the N_2-sorption isotherm for $CdSnO_3{\cdot}3H_2O$ prepared by the homogenous precipitation at pH 7, which exhibited stepwise adsorption and desorption (type-IV isotherm) and

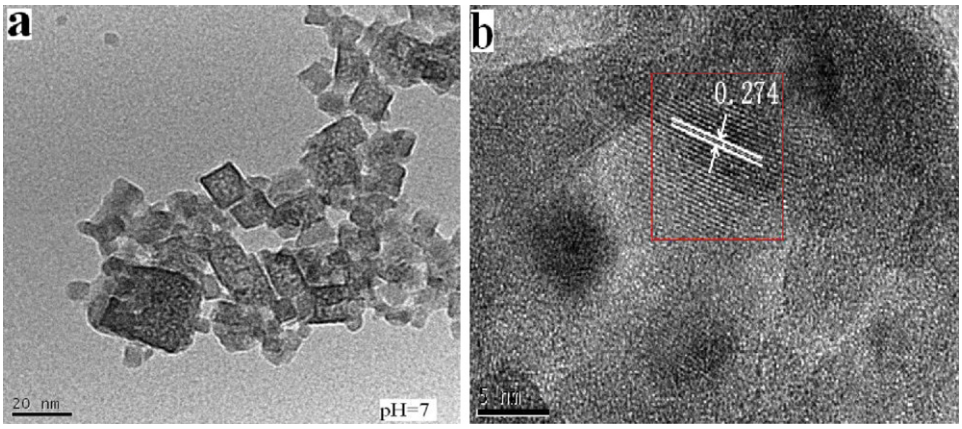

Fig. 2. (a) Typical TEM image of the $CdSnO_3 \cdot 3H_2O$ sample (pH 7) and (b) typical HRTEM image of the $CdSnO_3 \cdot 3H_2O$ sample.

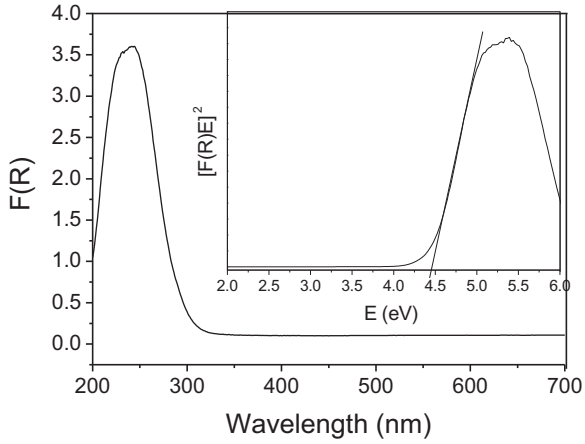

Fig. 3. The UV–vis diffuse reflectance spectrum of the samples and optical band gap energy (E_g) of $CdSnO_3 \cdot 3H_2O$ (inset) prepared at pH 7.

indicative of a mesoporous solid. The average pore size of the $CdSnO_3 \cdot 3H_2O$ was 6–8 nm, due to the accumulation of particles. The BET specific surface area of the sample calculated from N_2 isotherms at 77 K was 91.8 $m^2\,g^{-1}$, whereas that of Degussa P25 was 50 $m^2\,g^{-1}$. The N_2-sorption isotherm of other samples prepared under varies pH were showed in Fig. S4. The BET specific surface areas of other samples prepared under varies pH 6, 8, 9 were calculated in the same way, which were 96.6 $m^2\,g^{-1}$, 89.5 $m^2\,g^{-1}$, 60.9 $m^2\,g^{-1}$, respectively.

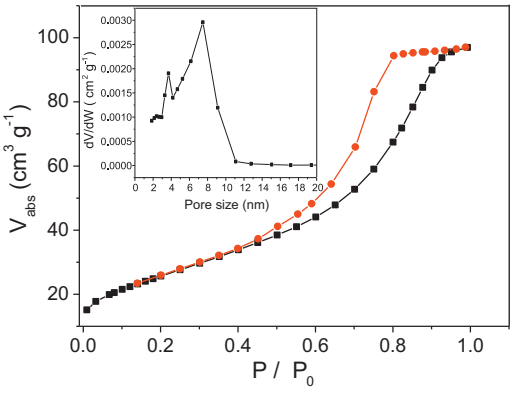

Fig. 4. Nitrogen adsorption–desorption isotherm and the pore size distribution plot for $CdSnO_3 \cdot 3H_2O$ (pH 7). The pore size distribution was estimated from the desorption branch of the isotherm.

3.2. Photocatalytic properties

Fig. 5 showed the photocatalytic activities of $CdSnO_3 \cdot 3H_2O$ samples synthesized at different pH values. The photocatalytic activities of samples for decomposing benzene in a continuous O_2 gas stream were evaluated under 254 nm ultraviolet light irradiation. The conversion ratios of benzene were respectively 20% and 25% for the $CdSnO_3 \cdot 3H_2O$ sample prepared at pH 6 and pH 9, and the production of CO_2 was about 300 and 200 ppm. The activity of

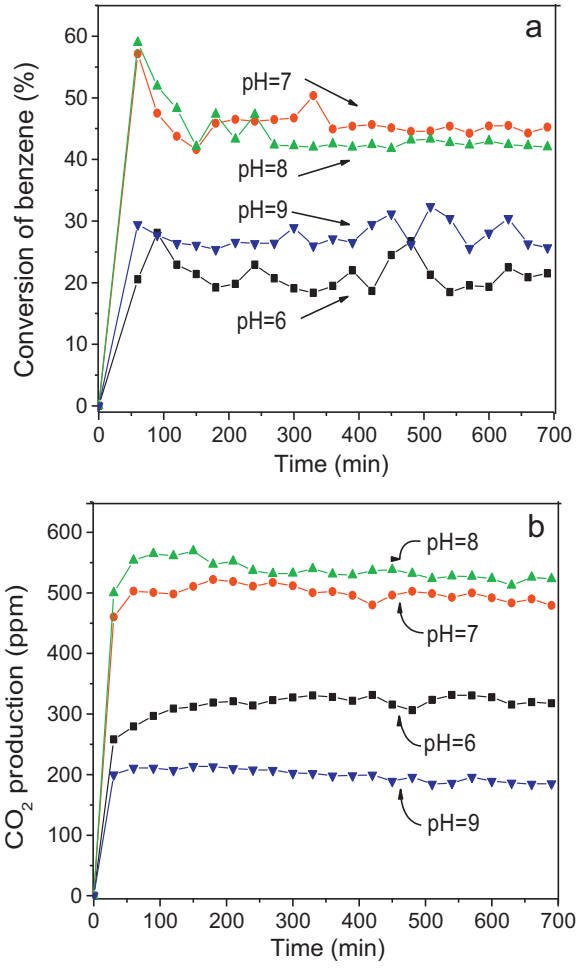

Fig. 5. Conversion of C_6H_6 (a) and the amount of produced CO_2 (b) over the $CdSnO_3 \cdot 3H_2O$ samples synthesized at different pH values.

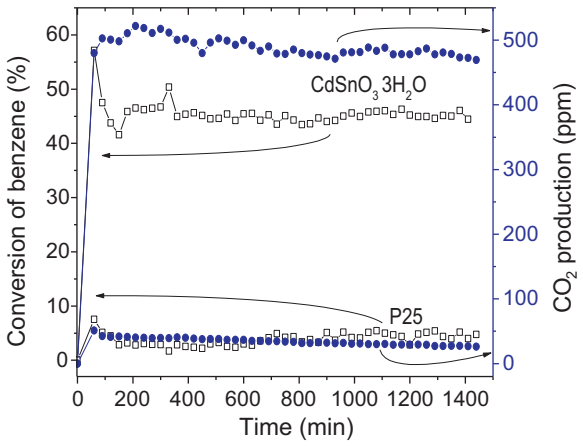

Fig. 6. Conversion of C_6H_6 and the amount of produced CO_2 over the $CdSnO_3{\cdot}3H_2O$ (pH 7) as a function of reaction time, with P25 as reference.

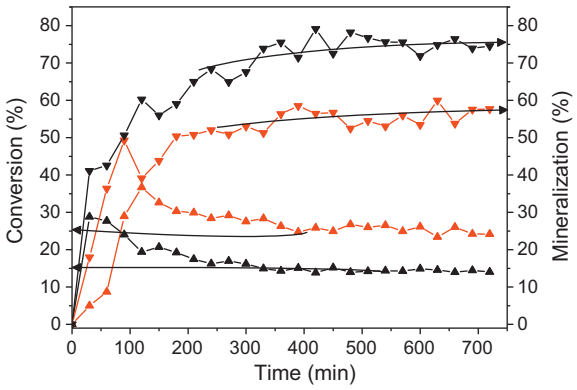

Fig. 7. Photooxidation of different volatile organic compounds (red mark is acetone and black mark is cyclothexane) in the presence of the new photocatalyst $CdSnO_3{\cdot}3H_2O$ under UV light. (For interpretation of the references to color in this figure legend, the reader is referred to the web version of the article.)

$CdSnO_3{\cdot}3H_2O$ synthesized at pH 7 or pH 8 was better, the conversion of benzene reached about 45% and 43% and the produced CO_2 were averagely 500 and 520 ppm, corresponding to the mineralization ratios of 60% and 66% respectively. Obviously, there were some other components, such as acetone which was detected as an intermediate of benzene photocatalytic degradation reported by Sitkiewitz and Heller [22], produced in the process of photocatalysis. So the best performing sample prepared at pH 7 was selected as a model for the follow-up study.

Fig. 6 showed the photodegradation of benzene over $CdSnO_3{\cdot}3H_2O$ and P25 under 254 nm UV light irradiation. For P25, the initial conversion ratio of benzene was about 5% and the amount of product CO_2 was 42 ppm corresponding to a mineralization ratio of 43%. However, during 24 h of P25 photocatalytic process, the conversion of benzene was maintained at about 5%, but the CO_2 production was reduced from 42 to 26 ppm, corresponding to the mineralization ratio decreased from 43% to 24%, and the color of the catalyst also changed from white to brown. The new photocatalyst $CdSnO_3{\cdot}3H_2O$ presented a much higher and stable activity during photocatalytic degradation of benzene under the same conditions. The conversion ratio of benzene was maintained stably at 45%, which was decuple of that of P25. The amount of product CO_2 was about 500 ppm, corresponding to the mineralization ratio of 60%. After 24 h of the photoreaction, the color changed from white to light yellow, which was different from the brown of P25 after reaction. This suggested that few carbons were accumulated on the surface of photocatalyst, which had no obvious influence on the surface activity sites of the photocatalyst and the $CdSnO_3{\cdot}3H_2O$ did not inactivate.The parallel experiment with SiO_2 catalyst as "blank test" was also performed to compare for the $CdSnO_3{\cdot}3H_2O$ photocatalyst during the photodegradation of benzene under UV light. As shown in Fig. S5, the negligible decomposition of benzene was observed at the same experimental condition. Other controlled experiments, either without the photocatalyst or with alpha-alumina under UV light irradiation had been investigated in our laboratory [17,23], showed that benzene cannot be photo-decomposed.

The photocatalytic activity of $CdSnO_3{\cdot}3H_2O$ was also evaluated by degradation of other organic compounds such as cyclohexane and acetone. As shown in Fig. 7, the efficient photocatalytic degradations of cyclohexane and acetone on $CdSnO_3{\cdot}3H_2O$ were observed. The conversion ratio of cyclohexane on $CdSnO_3{\cdot}3H_2O$ was 15%, but the mineralization ratio of cyclohexane on $CdSnO_3{\cdot}3H_2O$ was up to 75%. As to acetone, the conversion ratio was about 25%, and the mineralization ratio was about 58%. Obviously, the conversion of acetone and cyclohexane on $CdSnO_3{\cdot}3H_2O$ was lower than that of benzene, but the mineralization ratios of them were similar. The high mineralization ratio of cyclohexane and acetone further proves that the new photocatalyst is promising.

As we know, the stability of a photocatalyst is important to its application. To investigate the stability of the new photocatalyst, further XRD and XPS characterizations of the used and original samples have been done. Fig. 8 showed the XRD patterns of $CdSnO_3{\cdot}3H_2O$ before and after reaction. The position and the intensities of peaks were nearly the same, which indicated that the bulk phase of the photocatalyst was stable. It is well known that the deactivation of catalysts might occur on the surface in the photocatalytic reaction, so XPS was used to test their surface chemical shift. The detailed spectra for Cd3d and Sn3d were shown in Fig. 9. The binding energies of Cd3d and Sn3d before and after use were nearly the same. It illustrated that there were no change in the chemical state of Cd and Sn during photocatalytic process. The X-ray photoelectron survey spectra of $CdSnO_3{\cdot}3H_2O$ was shown in Fig. S6 (Supporting Information).

3.3. Photocatalytic mechanism

As described above, the new photocatalyst $CdSnO_3{\cdot}3H_2O$ presented a high activity on degradation of volatile organic compounds

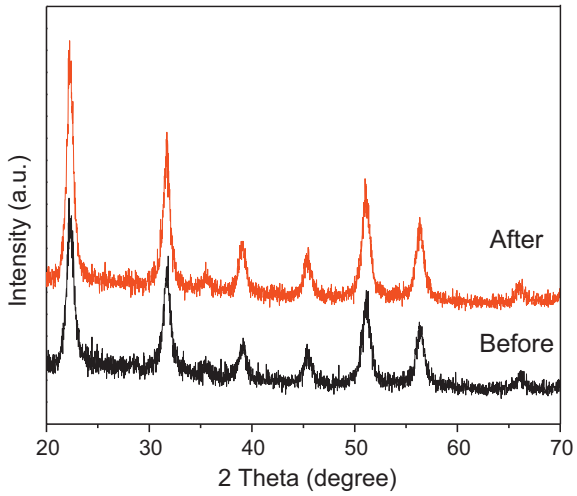

Fig. 8. The comparison of X-ray diffraction patterns of $CdSnO_3{\cdot}3H_2O$ before and after reaction.

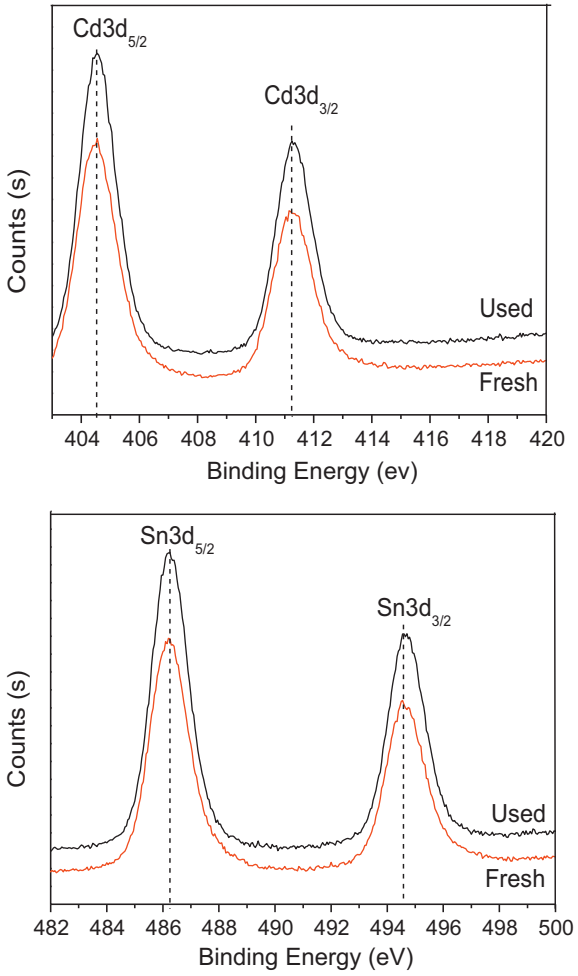

Fig. 9. High-resolution XPS spectra of $CdSnO_3{\cdot}3H_2O$ before and after reaction.

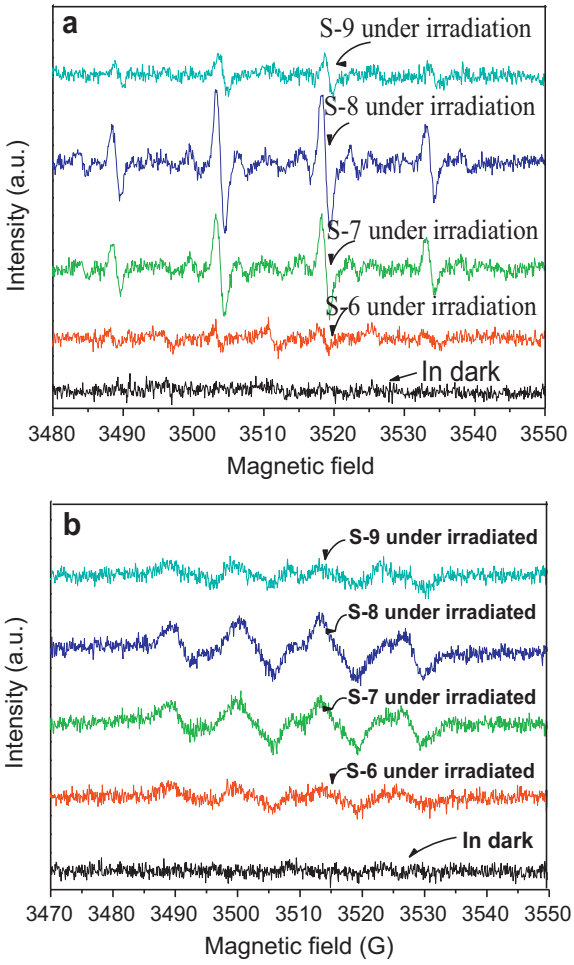

Fig. 10. ESR signals of the DMPO–•OH (a) and DMPO–O_2•$^-$ (b) in $CdSnO_3{\cdot}3H_2O$ system without irradiation and with irradiation (the S-6, S-7, S-8, S-9 corresponding to the sample synthesized at pH 6, 7, 8, 9), respectively.

under ambient condition, which could meet the demand of atmospheric environmental remediation. Understanding of the photocatalystic mechanism is also very important for its potential application. It is well known that the radical is a crucial factor related to the photoactivity of semiconductors, so the formation of radical on the new photocatalyst was discussed. When the $CdSnO_3{\cdot}3H_2O$ was irradiated by 254 UV light, it would generate pairs of highly reactive electrons and holes (R1). Then the trapping or recombination of the photo-generated electrons or holes would play significant roles in photocatalytic process. In generally, the electron was trapped and the hole subsequently oxidized the surface hydroxyl to form OH radical [24]. In practice, the process was complicated in various photocatalytic systems. The holes were possibly transferred to react with –OH and absorbed VOCs (R2, R3) [25]. In the presence of H_2O, the surface hydroxyl groups consumed in the photoreaction could be regenerated, which leads to a successive catalytic cycle [26]. This enhanced the separation of the pairs of electrons/holes and the formation of •OH radicals (R4). Simultaneously, the electrons were transferred to react with absorbed O_2 (R5, R6). The radicals diffused into the gas phase during the excitation of semiconductor in the presence of H_2O, which has been demonstrated by Guillaume Vincent [27,28]. Therefore, during the photocatalytic degradation of VOCs over $CdSnO_3{\cdot}3H_2O$, the production and consumption of electrons and holes were possibly following these reactions:

$$\text{Photocatalyst} + h\nu \rightarrow h^+ + e^- \quad \text{(R1)}$$

$$h^+ + {-OH} \rightarrow {^\bullet OH} \quad \text{(R2)}$$

$$h^+ + R_{VOCs} \rightarrow {^\bullet R^+}_{VOCs} \quad \text{(R3)}$$

$$h^+ + H_2O \rightarrow {^\bullet OH} + H^+ \quad \text{(R4)}$$

$$H^+ + O_2 + e^- \rightarrow {^\bullet O_2H} \quad \text{(R5)}$$

$$e^- + O_2 \rightarrow {^\bullet O_2}^- \quad \text{(R6)}$$

The generation of •OH, and $^\bullet O_2{}^-$ radicals was confirmed by the ESR spin trap with DMPO technique. As shown in Fig. 10, when $CdSnO_3{\cdot}3H_2O$ was illuminated with UV 254 nm light, four characteristic peaks of DMPO–•OH with intensity of 1:2:2:1 had been obviously observed in water suspension. No signals had been detected without UV irradiation. The abundance of −OH and H_2O on the new photocatalyst could accept photo-generated holes to yield highly reactive •OH radicals (as R2, R4), which improved the separation of electrons and holes. The separated electrons were transferred and reacted with absorbed O_2 and formed $^\bullet O_2{}^-$. As shown in Fig. 10b, six characteristic peaks of DMPO–$^\bullet O_2{}^-$ adduct had been also obviously observed in methanol dispersions. Based on the above discussion, focusing on the electron–hole transfer process and the role of the hydroxyl groups or water on the new photocatalyst, the following reaction mechanism was proposed. When $CdSnO_3{\cdot}3H_2O$ was efficiently excited to produce electron/hole pairs under

254 nm UV light irradiation, the water on the new photocatalyst prohibited the recombination of photo-generated carriers and played an important role on the formation of reactive oxygenated species. The more $^{\bullet}OH$, and $^{\bullet}O_2^-$ radicals produced, the higher photocatalytic performance of the new photocatalyst $CdSnO_3{\cdot}3H_2O$ toward VOCs under UV light at ambient condition was obtained.

In general, the activity of a photocatalyst is usually influenced by many factors. Besides the separation ratio of photogenerated electron/hole pairs and their transportation rate on the catalyst, the surface area and the photoabsorption ability also greatly influence the overall activity of photocatalyst [29]. The larger BET surface area the $CdSnO_3{\cdot}3H_2O$ was, the more surface active sites emerged. The adsorbed reactive species had more chance to react with adsorbed organic compounds [30]. For example, the $CdSnO_3{\cdot}3H_2O$ synthesized at pH 7 or 8 had a large BET surface area (about $90\,m^2\,g^{-1}$) which leads to the more chance of the reactive oxygenated species reacting with absorbed benzene. Their overall activities were higher than the sample synthesized at pH 9. As to the sample synthesized at pH 6, the BET surface area was $96.6\,m^2\,g^{-1}$, but the absorption ability of light was poorer than the samples synthesized at pH 7, 8 (as shown in Fig. S3), which leads to its lower photocatalytic activity. In addition, the ESR results in Fig. 10 showed that, the signal intensities of DMPO–$^{\bullet}OH$ and DMPO–$O_2^{\bullet-}$ in the $CdSnO_3{\cdot}3H_2O$ synthesized at pH 7, 8 were stronger than the samples synthesized at pH 6, 9, which also confirmed that the performance of photocatalyst would be influenced by the different characterization of samples synthesized at different conditions.

4. Conclusions

A new photocatalyst $CdSnO_3{\cdot}3H_2O$ nanocubes with the sizes of 10–20 nm have been prepared successfully via a facile homogenous precipitation method for the first time. This new binary metal hydrate semiconductor presented a better photocatalytic performance toward benzene than TiO_2. Due to its high photocatalytic mineralization of the VOCs and its simple synthesis method, the $CdSnO_3{\cdot}3H_2O$ and other metal hydrates would be further study in the environmental application.

Acknowledgments

This work was financially supported by the National Natural Science Foundation of China (21173047, 21073036 and 21033003), and National Basic Research Program of China (973 Program, 2013CB632405).

Appendix A. Supplementary data

Supplementary data associated with this article can be found, in the online version, at http://dx.doi.org/10.1016/j.apcatb.2012.09.030.

References

[1] M.R. Hoffmann, S.T. Martin, W. Choi, D.W. Bahnemann, Chemical Reviews 95 (1995) 69–96.
[2] A. Fujishima, T.N. Rao, D.A. Tryk, Journal of Photochemistry and Photobiology C: Photochemistry Review 1 (2000) 1–21.
[3] R. Mendez-Roman, N. Cardona-Martinez, Catalysis Today 40 (1998) 353–365.
[4] G. Martra, S. Coluccia, L. Marchese, V. Augugliaro, V. Loddo, L. Palmisano, M. Schiavello, Catalysis Today 53 (1999) 695–702.
[5] S.U.M. Khan, M. Al-Shahry, W.B. Ingler, Science 297 (2002) 2243–2245.
[6] S. Kim, S.J. Hwang, W.Y. Choi, Journal of Physical Chemistry B 109 (2005) 24260–24267.
[7] N.N. Lichtin, M.J. Sadeghi, Photochemistry and Photobiology A 113 (1998) 81–88.
[8] H. Einaga, S. Futamura, T. Ibusuki, Physical Chemistry Chemical Physics 1 (1999) 4903–4908.
[9] A. Kudo, K. Omori, H.J. Kato, American Chemical Society 121 (1999) 11459–11467.
[10] S. Mahapatra, G. Madras, T.N.G. Row, Journal of Physical Chemistry C 111 (2007) 6505–6511.
[11] B. Zhou, X. Zhao, H.J. Liu, J.H. Qu, C.P. Huang, Applied Catalysis B: Environmental 99 (2010) 214–221.
[12] Y.D. Hou, X.C. Wang, L. Wu, Z.X. Ding, X.Z. Fu, Environmental Science and Technology 40 (2006) 5799–5803.
[13] H. Xue, Z.H. Li, L. Wu, Z.X. Ding, X.X. Wang, X.Z. Fu, Journal of Physical Chemistry C 112 (2008) 5850–5855.
[14] X.D. Lou, X.H. Jia, J.Q. Xu, S.Z. Liu, Q.H. Gao, Materials Science and Engineering A 432 (2006) 221–225.
[15] W.J. Wang, J.H. Bi, L. Wu, Z.H. Li, X.Z. Fu, Scripta Materialia 60 (2009) 186–189.
[16] X.L. Fu, X.X. Wang, Z.X. Ding, Applied Catalysis B: Environmental 91 (2009) 67–72.
[17] T.J. Yan, J.L. Long, Y.S. Chen, X.X. Wang, Comptes Rendus Chimie 11 (2008) 101–106.
[18] Z.H. Li, Z.P. Xie, Y.F. Zhang, The Journal of Physical Chemistry C 111 (2007) 18348–18352.
[19] M. Sun, D.Z. Li, Y.B. Chen, W. Chen, W.J. Li, Y.H. He, X.Z. Fu, Journal of Physical Chemistry C 113 (2009) 13825–13831.
[20] Y.W. Tang, Y. Jiang, Z.Y. Jia, Inorganic Chemistry 45 (2006) 10774–10779.
[21] M.A. Butler, Journal of Applied Physics 48 (1977) 1914–1920.
[22] S. Sitkiewitz, A. Heller, New Journal of Chemistry 20 (1996) 233–241.
[23] Y.D. Hou, L. Wu, X.C. Wang, Z.X. Ding, Z.H. Li, X.Z. Fu, Journal of Catalysis 250 (2007) 12–18.
[24] M. Anpo, T. Shima, Y. Kubokawa, Chemistry Letters 12 (1985) 1799–1802.
[25] O. d'Hennezel, P. Pichat, D.F. Ollis, Journal of Photochemistry and Photobiology A 118 (1998) 197–204.
[26] V. Keller, P. Bernhardt, F. Garin, Journal of Catalysis 215 (2003) 129–138.
[27] G. Vincent, A. Aluculesei, A. Parker, C. Fittschen, O. Zahraa, P.M. Marquaire, Journal of Physical Chemistry C 112 (2008) 9115–9119.
[28] J. Thiebaud, F. Thevenet, C. Fittschen, Journal of Physical Chemistry C 114 (2010) 3082–3088.
[29] W.K. Chang, K.K. Rao, H.C. Kuo, J.F. Cai, M.S. Wong, Applied Catalysis A 321 (2007) 1–6.
[30] Y. Shiraishi, T. Hirai, Journal of Photochemical and Photobiology C 9 (2008) 157–170.